Langmuir Article

pubs.acs.org/Langmuir
© 2010 American Chemical Society

Nanoparticle Formation and Ultrathin Film Electrodeposition of Carbazole Dendronized Polynorbornenes Prepared by Ring-Opening Metathesis Polymerization

Guoqian Jiang, Ramakrishna Ponnapati, Roderick Pernites, Carlos D. Grande,[†] Mary Jane Felipe, Edward Foster, and Rigoberto Advincula*

Department of Chemistry and Department of Chemical and Biomolecular Engineering, University of Houston Houston, Texas 77204-5003, United States. [†]Present address: Departamento de Quimica, Universidad del Valle, A.A. 25360, Cali, Colombia.

Received August 29, 2010. Revised Manuscript Received September 24, 2010

We report on the synthesis, electropolymerization, and nanoparticle formation of a series of electroactive carbazole-terminated dendronized linear polynorbornenes prepared by living ring-opening metathesis polymerization (ROMP). The molecular weight (MW) of the dendronized polymers was controlled by varying the feed ratio between the dendronized monomer and first-generation Grubbs' catalyst. Ultrathin films were prepared by electrodeposition. The electrochemical behavior and viscoelastic properties of such films were found to be highly dependent on the dendron generation and linear polymer MW as studied by electrochemical quartz crystal microbalance (E-QCM). Moreover, nanoparticle formation and size/shape control were observed by tuning the surface wetting properties of the substrate during adsorption and by intramolecular cross-linking via chemical oxidation in solution.

1. Introduction

Dendronized linear polymers (DLPs) are a class of macromolecules with a linear main chain and branched dendron side groups.[1−6] A variety of pendant functionalities and tunable architectures of DLPs offer interesting physicochemical properties with a number of possible applications.[2,7−14] Dendronized linear polymers can be synthesized via different strategies including convergent,[12,15−17] divergent,[18,19] and macromonomer approaches.[20,21] The latter refers to the use of dendronized monomers, followed by polymerization to form the main chain. Due to high steric bulking of higher generation dendrons around the main chain, this polymerization process sometimes yields low molecular weight (M_w or M_n) products.[4,22] When the size of dendrons reaches a threshold point, they are densely packed around the polymer backbone, forcing it to stretch out in the form of "molecular cylinders". These rodlike macromolecules with sufficiently long architecture can be directly visualized and manipulated by scanning probe microscopy (SPM) techniques.[4,23−27] Recently, the Frechet group synthesized dendronized diblock copolymers via ring-opening metathesis polymerization (ROMP). The length of the ester and aryl ether dendron blocks and the nature of the dendron wedges allowed nanostructure control as visualized by atomic force microscopy (AFM).[27] More recently, they reported the preparation of cyclic organo-nanostructure via ring-expansion metathesis polymerization of a dendronized macromonomer.[28] This route should enable new nanoscale macromolecular objects with well-defined shapes and dimensions.

ROMP has been one of the most useful methods in polymer synthesis including formation of highly branched polymers. As a novel living/controlled polymerization method, ROMP has

*To whom correspondence should be addressed. E-mail: radvincula@uh.edu.

(1) Hawker, C. J.; Fréchet, J. M. J. *Polymer* **1992**, *33*, 1507.
(2) Schluter, A. D.; Rabe, J. P. *Angew. Chem., Int. Ed.* **2000**, *39*, 864.
(3) Zhang, A. F.; Shu, L. J.; Bo, Z. S.; Schluter, A. D. *Macromol. Chem. Phys.* **2003**, *204*, 328.
(4) Helms, B.; Mynar, J. L.; Hawker, C. J.; Frechet, J. M. J. *J. Am. Chem. Soc.* **2004**, *126*, 15020.
(5) Frauenrath, H. *Prog. Polym. Sci.* **2005**, *30*, 325.
(6) Percec, V.; Rudick, J. G.; Peterca, M.; Wagner, M.; Obata, M.; Mitchell, C. M.; Cho, W. D.; Balagurusamy, V. S. K.; Heiney, P. A. *J. Am. Chem. Soc.* **2005**, *127*, 15257.
(7) Gossl, I.; Shu, L.; Schluter, A. D.; Rabe, J. P. *J. Am. Chem. Soc.* **2002**, *124*, 6860.
(8) Luo, J. D.; Liu, S.; Haller, M.; Liu, L.; Ma, H.; Jen, A. K. Y. *Adv. Mater.* **2002**, *14*, 1763.
(9) Liang, C. O.; Helms, B.; Hawker, C. J.; Frechet, J. M. J. *Chem. Commun.* **2003**, *20*, 2524.
(10) Fu, Y. Q.; Li, Y.; Li, J.; Yan, S.; Bo, Z. S. *Macromolecules* **2004**, *37*, 6395.
(11) Wu, C. W.; Sung, H. H.; Lin, H. C. *J. Polym. Sci., Polym. Chem.* **2006**, *44*, 6765.
(12) Lee, C. C.; Frechet, J. M. J. *Macromolecules* **2006**, *39*, 476.
(13) Percec, V.; Rudick, J. G.; Peterca, M.; Heiney, P. A. *J. Am. Chem. Soc.* **2008**, *130*, 7503.
(14) Li, W.; Zhang, A.; Feldman, K.; Walde, P.; Schlüter, A. D. *Macromolecules* **2008**, *41*, 3659.
(15) Lijin, S.; Schafer, A.; Schluter, A. D. *Macromolecules* **2000**, *33*, 4321.
(16) Grayson, S. M.; Frechet, J. M. J. *Macromolecules* **2001**, *34*, 6542.
(17) Yoshida, M.; Fresco, Z. M.; Ohnishi, S.; Frechet, J. M. J. *Macromolecules* **2005**, *38*, 334.
(18) Karakaya, B.; Claussen, W.; Gessler, K.; Saenger, W.; Schluter, A. D. *J. Am. Chem. Soc.* **1997**, *119*, 3296.
(19) Mynar, J. L.; Choi, T.-L.; Yoshida, M.; Victor, K.; Hawker, C. J.; Frechet, J. M. J. *Chem. Commun.* **2005**, 5169.
(20) Lubbert, A.; Nguyen, T. Q.; Sun, F.; Sheiko, S. S.; Klok, H.-A. *Macromolecules* **2005**, *38*, 2064.
(21) Nystrom, A.; Malkoch, M.; Furo, I.; Nystrom, D.; Unal, K.; Antoni, P.; Vamvounis, G.; Hawker, C. J.; Wooley, K.; Malmstrom, E.; Hult, A. *Macromolecules* **2006**, *39*, 7241.
(22) Scrivanti, A.; Fasan, S.; Matteoli, U.; Seraglia, R.; Chessa, G. *Macromol. Chem. Phys.* **2000**, *201*, 326.
(23) Shu, L.; Schluter, A. D.; Ecker, C.; Severin, N.; Rabe, J. P. *Angew. Chem., Int. Ed.* **2001**, *40*, 4666.
(24) Kim, K. T.; Han, J.; Ryu, C. Y.; Sun, F. C.; Sheiko, S. S.; Winnik, M. A.; Manners, I. *Macromolecules* **2006**, *39*, 7922.
(25) Pyun, J.; Tang, C.; Kowalewski, T.; Frechet, J. M. J.; Hawker, C. J. *Macromolecules* **2005**, *38*, 2674.
(26) Ostmark, E.; Harrisson, S.; Wooley, K. L.; Malmstrom, E. E. *Biomacromolecules* **2007**, *8*, 1138.
(27) Rajaram, S.; Choi, T.-L.; Rolandi, M.; Frechet, J. M. J. *J. Am. Chem. Soc.* **2007**, *129*, 9619.
(28) Boydston, A. J.; Holcombe, T. W.; Unruh, D. A.; Frechet, J. M. J.; Grubbs, R. H. *J. Am. Chem. Soc.* **2009**, *131*, 5388.

Scheme 1. Synthesis Route for the Dendronized Linear Polynorbornenes with the Carbazole Dendrons (G0, G1, and G2) Pendant Groups Using Grubbs' Generation I Catalyst

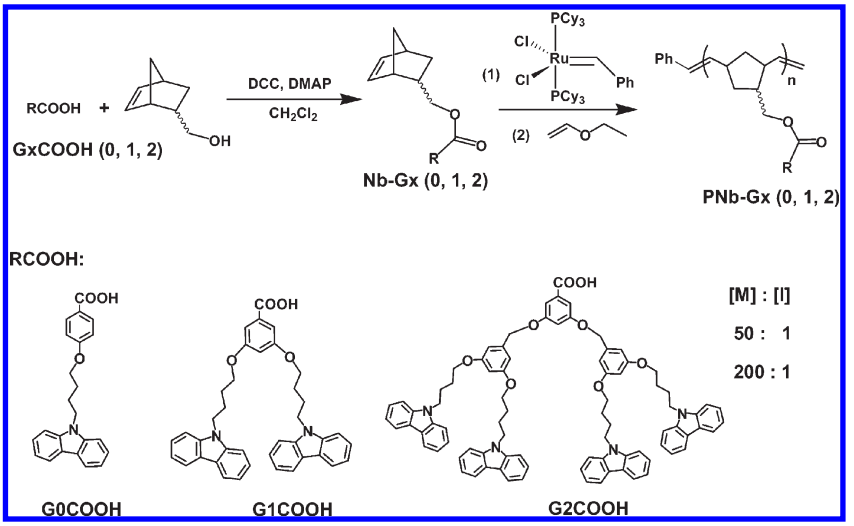

attracted increasing interest over the past two decades.[29−33] The ring structured units with high strain energy, such as norbornene, are typically employed as the focal point for polymerizability. In the presence of the highly reactive transition metal catalysts, the relief of the ring strain affords various polymer architectures with specified molecular weights (MWs) and narrow polydispersity indices (PDIs). As developed by Grubbs and co-workers, the late transition metal catalysts, especially ruthenium (Ru)-based carbene derivatives, provide many advantages including fast initiation rate, functional-group tolerance, and high activity.[34−39]

Polycarbazoles or polymers grafted with carbazole (Cbz) as pendants have been widely applied in the fabrication of electroluminescent devices,[40−42] photorefractive materials,[43,44] electrochromic materials,[45,46] and memory devices.[47] In our group, carbazole containing polymers have been synthesized and studied for various macromolecular architectures and device applications.[48−54] In all the above applications, the use of carbazole derivatized polymers in light emitting diodes (LEDs) offers efficient hole transporting properties, good solution processability, and high thermal stability.[55−58] Electronically conducting materials based on π-conjugated organic polymers[59] have received extensive interest over several decades on a wide range of applications.[60] Of recent interest are applications in nanoelectronics or nano-object formation.[61,67] Previous studies have been reported on the interesting properties of conjugated polymers and dendrimers as nano-objects.[62] Using the precursor polymer approach, cross-linking of side chain electroactive functional groups upon chemical/electrochemical oxidation leads to the formation of conjugated polymer networks (CPNs).[63,64] Different electroactive functional groups have been attached to nonconjugated and conjugated polymer backbones followed by cross-linking.[49,50,53,65,66] CPN formation has also been applied to dendrimeric precursors forming shape-persistent conjugated nanoparticles and nano-objects.[67,68] Other previous works have addressed the significance and interest on polynorbornenes with electroactive functional side groups.[63,69−71] However, to the best of our knowledge, no group has reported the

(29) Nguyen, S. T.; Johnson, L. K.; Grubbs, R. H.; Ziller, J. W. *J. Am. Chem. Soc.* **1992**, *114*, 3974.
(30) Bielawski, C. W.; Grubbs, R. H. *Angew. Chem., Int. Ed.* **2000**, *39*, 2903.
(31) Schrock, R. R. *Tetrahedron* **1999**, *55*, 8141.
(32) Slugovc, C. *Macromol. Rapid Commun.* **2004**, *25*, 1283.
(33) Bielawski, C. W.; Grubbs, R. H. *Prog. Polym. Sci.* **2007**, *32*, 1.
(34) Trnka, T. M.; Grubbs, R. H. *Acc. Chem. Res.* **2001**, *34*, 18.
(35) Trnka, T. M.; Morgan, J. P.; Sanford, M. S.; Wilhelm, T. E.; Scholl, M.; Choi, T.-L.; Ding, S.; Day, M. W.; Grubbs, R. H. *J. Am. Chem. Soc.* **2003**, *125*, 2546.
(36) Grubbs, R. H. *Angew. Chem., Int. Ed.* **2006**, *45*, 3760.
(37) Choi, T. L.; Grubbs, R. H. *Angew. Chem., Int. Ed.* **2003**, *42*, 1743.
(38) Yang, L. R.; Mayr, M.; Wurst, K.; Buchmeiser, M. R. *Chem.—Eur. J.* **2004**, *10*, 5761.
(39) Gstrein, X.; Burtscher, D.; Szadkowska, A.; Barbasiewicz, M.; Stelzer, F.; Grela, K.; Slugovc, C. *J. Polym. Sci., Polym. Chem.* **2007**, *45*, 3494.
(40) Romero, B.; Schaer, M.; Leclerc, M.; Ades, D.; Siove, A.; Zuppiroli, L. *Synth. Met.* **1996**, *80*, 271.
(41) Peng, Z. H.; Bao, Z. N.; Galvin, M. E. *Chem. Mater.* **1998**, *10*, 2086.
(42) van Dijken, A.; Bastiaansen, J. J. A. M.; Kiggen, N. M. M.; Langeveld, B. M. W.; Rothe, C.; Monkman, A.; Bach, I.; Stossel, P.; Brunner, K. *J. Am. Chem. Soc.* **2004**, *126*, 7718.
(43) Kippelen, B.; Tamura, K.; Peyghambarian, N.; Padias, A. B.; Hall, H. K. *Phys. Rev. B* **1993**, *48*, 10710.
(44) Zhang, Y. D.; Wada, T.; Sasabe, H. *J. Mater. Chem.* **1998**, *8*, 809.
(45) Schwendeman, I.; Hickman, R.; Sonmez, G.; Schottland, P.; Zong, K.; Welsh, D. M.; Reynolds, J. R. *Chem. Mater.* **2002**, *14*, 3118.
(46) Witker, D.; Reynolds, J. R. *Macromolecules* **2005**, *38*, 7636.
(47) Ling, Q. D.; Song, Y.; Ding, S. J.; Zhu, C. X.; Chan, D. S. H.; Kwong, D. L.; Kang, E. T.; Neoh, K. G. *Adv. Mater.* **2005**, *17*, 455.
(48) Xia, C. J.; Advincula, R. C. *Macromolecules* **2001**, *34*, 5854.
(49) Baba, A.; Onishi, K.; Knoll, W.; Advincula, R. C. *J. Phys. Chem. B* **2004**, *108*, 18949.
(50) Taranekar, P.; Baba, A.; Fulghum, T. M.; Advincula, R. *Macromolecules* **2005**, *38*, 3679.
(51) Fulghum, T.; Karim, S. M. A.; Baba, A.; Taranekar, P.; Nakai, T.; Masuda, T.; Advincula, R. C. *Macromolecules* **2006**, *39*, 1467.
(52) Waenkaew, P.; Taranekar, P.; Phanichphant, P.; Advincula, R. *Macrom. Rapid Commun.* **2007**, *28*, 1522.
(53) Taranekar, P.; Fulghum, T.; Baba, A.; Patton, D.; Advincula, R. *Langmuir* **2007**, *23*, 908.
(54) Huang, C.; Jiang, G.; Advincula, R. *Macromolecules* **2008**, *41*, 4661.
(55) Thomas, K. R. J.; Lin, J. T.; Tao, Y. T.; Ko, C. W. *J. Am. Chem. Soc.* **2001**, *123*, 9404.
(56) Liu, B.; Yu, W.-L.; Lai, Y.-H.; Huang, W. *Chem. Mater.* **2001**, *13*, 1984.
(57) Li, Y.; Ding, J.; Day, M.; Tao, Y.; Lu, J.; D'iorio, M. *Chem. Mater.* **2004**, *16*, 2165.
(58) Morin, J. F.; Leclerc, M.; Ades, D.; Siove, A. *Macromol. Rapid Commun.* **2005**, *26*, 761.
(59) Chiang, C. K.; Fincher, C. R.; Park, Y. W.; Heeger, A. J.; Shirakawa, H.; Louis, E. J.; Gau, S. C.; MacDiarmid, A. G. *Phys. Rev. Lett.* **1977**, *39*, 1098.
(60) Argun, A. A.; Aubert, P. H.; Thompson, B. C.; Schwendeman, I.; Gaupp, C. L.; Hwang, J.; Pinto, N. J.; Tanner, D. B.; MacDiarmid, A. G.; Reynolds, J. R. *Chem. Mater.* **2004**, *16*, 4401.
(61) Zhu, Y.; Champion, R. D.; Jenekhe, S. A. *Macromolecules* **2006**, *39*, 8712.
(62) Schenning, A. P. H. J.; Meijer, E. W. *Chem. Commun.* **2005**, *26*, 3245.
(63) Jang, S. Y.; Sotzing, G. A.; Marquez, M. *Macromolecules* **2002**, *35*, 7293.
(64) Weder, C. *Chem. Commun.* **2005**, *43*, 5378.
(65) Xia, C.; Fan, X. W.; Park, M. K.; Advincula, R. C. *Langmuir* **2001**, *17*, 7893.
(66) Taranekar, P.; Fan, X. W.; Advincula, R. *Langmuir* **2002**, *18*, 7943.
(67) Taranekar, P.; Park, J.-Y.; Fulghum, T.; Patton, D.; Advincula, R. *Adv. Mater.* **2006**, *18*, 2461.
(68) Taranekar, P.; Fulghum, T.; Patton, D.; Ponnapati, R.; Clyde, G.; Advincula, R. *J. Am. Chem. Soc.* **2007**, *129*, 12537.
(69) Stepp, B. R.; Nguyen, S. T. *Macromolecules* **2004**, *37*, 8222.
(70) Jang, S.-Y.; Marquez, M.; Sotzing, G. A. *J. Am. Chem. Soc.* **2004**, *126*, 9476.

use of generational dendrons with electroactive carbazole peripheral groups for polymerization using ROMP.

In this work, linear polynorbornenes with different architectures were synthesized via ROMP using the first-generation Grubbs' catalyst (Scheme 1). The Frechet-type dendrons with carbazole terminal groups of different generations (G0, G1, and G2) were attached to norbornenyl methanol to form dendrons for metathesis polymerization. The polymers were then characterized by NMR, GPC, TGA, and DSC. Electrochemical quartz crystal microbalance (E-QCM) was employed to study the electrochemical cross-linking behavior and thin film deposition onto gold electrodes. The electrochemically deposited films were examined by AFM. Nanoparticle formation was observed with controlled adsorption on wetting and nonwetting substrates. In particular, a high generation carbazole dendronized polynorbornene with a longer chain length, PNbG2-200, was spin coated onto mica and gold substrates with hydrophilic and hydrophobic surfaces. The size and shape control of the nano-objects was investigated, which may be an attractive feature for potential applications as conducting polymer nanoparticles and nano-objects.

2. Experimental Section

2. 1. Materials. All materials, solvents, deuterated solvents, and reagents were purchased from either Aldrich, VWR, or Acros Organics and used without further purification. Dichloromethane and tetrahydrofuran (THF) were dried over CaH_2 and sodium benzophenone ketyl, respectively, and used directly before the reactions or any measurements.

2.2. Instrumentation. Nuclear magnetic resonance (NMR) spectra were recorded on a General Electric QE-300 spectrometer operating at 300 MHz for ^{1}H NMR and 75 MHz for ^{13}C NMR. UV−vis spectra were recorded using an Agilent 8453 spectrometer. Matrix assisted laser desorption ionization time-of-flight (MALDI-TOF) analysis was performed on a Voyager DE-STR system from Applied Biosystems. A high voltage of 20 KV, pulse rate of 20 Hz, and N_2 laser (337 nm) were used to probe the sample mass. Gel permeation chromatography (GPC) was carried out with a Viscotek 270 apparatus with a triple detector array (RALS, IV, RI, or UV) equipped with 2 GMHHR-M and 1 GMHHR-L mixed bed ViscoGel columns with THF as eluent at a flow rate of 1 mL/min. A Viscotek VE 1122 GPC solvent pump, a Viscotek VE 7510 GPC degasser, and Viscotek TriSEC software were also used. The thermal properties of the polymers were measured by thermogravimetric analysis (TGA) on a TA Instruments TGA 2920 apparatus. The samples were heated up to 800 °C at a heating rate of 10 °C/min under a dry nitrogen atmosphere (flow rate 80 mL/min) on a TA Instruments 2950 thermogravimetric analyzer. T_g was determined by differential scanning calorimetry (DSC) from the midpoint of the inflection tangent from the second heating at 5 °C/min. TGA and DSC data were analyzed using TA Instruments' Universal Analysis software. The QCM apparatus, probe, and crystals are available from MAXTEK Inc. (now Inficon Corp.). The data acquisition was done using an RQCM (research quartz crystal microbalance, MAXTEK, Inc.) system equipped with a built-in phase lock oscillator and the RQCM Data-Log software. This was coupled with the Amel potentiostat to generate EC-QCM results. A 5 MHz AT-cut Au-coated quartz crystal with an effective area of 1.327 cm^2 was used as a working electrode. Platinum as a counter electrode and Ag/AgCl wire were used as a reference to measure in situ polymerization during cyclic voltammetry (CV) experiments. To initiate the experiment, an inert probe was first immersed in methylene chloride until a stable frequency was obtained. AFM imaging was examined in ambient conditions with a PicoSPM II (PicoPlus, Molecular Imaging, now Agilent Technologies) instrument in the tapping mode.

(71) Zhao, C.; Zhang, Y.; Wang, C.; Rothberg, L.; Ng, M.-K. *Org. Lett.* **2006**, *8*, 1585.

2.3. Synthesis of Terminal Carbazole Dendron Monomers. The carbazole dendron carboxylic acids (G0COOH, G1COOH, and G2COOH) were synthesized according to earlier reports.[68,72]

Synthesis of Bicyclo[2.2.1]hept-5-en-2-ylmethyl 4-(4-(9H-Carbazol-9-yl)butoxy)benzoate (*Nb-G0*). In a 100 mL round-bottom flask equipped with a stir bar and an addition funnel, a solution of G0COOH (1.28 g, 3.56 mmol), 5-norbornene-2-methanol (mixture of endo and exo) (0.53 g, 4.28 mmol), and 4-(dimethylamino)pyridine (DMAP) (44 mg, 0.360 mmol) in 40 mL of dry CH_2Cl_2 was cooled to 0 °C under N_2. Dicyclohexylcarbodiimide (DCC) (0.883 g, 4.28 mmol) was dissolved in 10 mL of CH_2Cl_2 and added dropwise to the reaction flask under stirring. After complete addition of DCC, the reaction was stirred for 10 min at 0 °C and then allowed to stir at room temperature overnight. Then, the white solids were removed by gravity filtration, and the filtrate was washed with dilute sodium bicarbonate (40 mL) and water (2 × 30 mL) and finally dried over anhydrous Na_2SO_4. The solution was filtered, and the solvent was removed to yield the white crude product mixture, which was further purified by column chromatography on silica gel using 4:1 CH_2Cl_2/hexane as the eluent. The final yield was 1.36 g (82.1%). ^{1}H NMR (300 MHz, $CDCl_3$, ppm): δ 8.10 (d, 2H, J = 7.5 Hz), 7.97 (dd, 2H, J = 9.0, 4.4 Hz), 7.36−7.51 (m, 4H), 7.19−7.27 (m, 2H), 6.85 (d, 2H, J = 9.0 Hz), 6.18 (q, 0.6 H, J = 3.0 Hz), 6.10 (m, 0.8 H), 5.98 (q, 0.6 H, J = 3.0 Hz), 4.40 (t, 4H, J = 6.9 Hz), 4.16 (dd, 0.6H, J = 9.0, 10.8 Hz), 4.08 (dd, 0.8H, J = 6.0, 9.3 Hz), 3.96 (t, 2H, J = 6.0 Hz), 3.84 (dd, 0.6H, J = 9.0, 10.8 Hz), 2.96 (s, 0.6H), 2.84 (s, 0.9H), 2.79 (s, 0.4H), 2.52 (m, 0.7H), 2.09 (m, 2H), 1.85 (m, 3H), 1.33 (m, 4H), 0.88 (m, 0.7H), 0.63 (m, 0.7H). ^{13}C NMR (75 MHz, $CDCl_3$, ppm): δ 172.2, 166.4, 166.3, 162.6, 162.5, 140.3, 137.6, 137.0, 136.3, 132.3, 131.6, 125.7, 123.0, 122.9, 120.4, 118.9, 114.0, 108.6, 95.0, 68.7, 68.1, 67.6, 53.5, 49.4, 45.0, 44.0, 43.7, 42.7, 42.2, 41.6, 38.1, 37.9, 29.7, 29.6, 29.0, 26.9, 25.8. MS (MALDI-TOF) Calcd. for $[C_{31}H_{31}NO_3]^+$: m/z 465.23. Found: m/z 465.49 $[M + H]^+$.

Synthesis of Bicyclo[2.2.1]hept-5-en-2-ylmethyl 3,5-Bis-(4-(9H-carbazol-9-yl) butoxy)benzoate (*Nb-G1*). In a 100 mL round-bottom flask equipped with a stir bar and an addition funnel, a solution of G1COOH (1.93 g, 3.23 mmol), 5-norbornene-2-methanol (mixture of endo and exo) (0.48 g, 3.88 mmol), and DMAP (40 mg, 0.323 mmol) in 40 mL of dry CH_2Cl_2 was cooled to 0 °C under N_2. DCC (0.800 g, 3.88 mmol) was dissolved in 10 mL of CH_2Cl_2 and added dropwise to the reaction flask under stirring. After complete addition of DCC, the reaction was stirred for 10 min at 0 °C and then allowed to stir at room temperature overnight. Then, the white solids were removed by gravity filtration, and the filtrate was washed with dilute sodium bicarbonate (40 mL) and water (2 × 30 mL) and finally dried over anhydrous Na_2SO_4. The solution was filtered, and the solvent was removed to yield the white crude product mixture, which was further purified by column chromatography on silica gel using 4:1 CH_2Cl_2/hexane as the eluent. The final yield was 1.58 g (69.6%). ^{1}H NMR (300 MHz, $CDCl_3$, ppm): δ 8.15 (d, 4H, J = 7.8 Hz), 7.39−7.57 (m, 8H), 7.20−7.34 (m, 6H), 6.60 (t, 1H, J = 2.1 Hz), 6.25 (q, 0.6 H, J = 3.0 Hz), 6.17 (m, 0.8 H), 6.06 (q, 0.6 H, J = 3.0 Hz), 4.46 (dd, 0.5H, J = 6.9 Hz), 4.37 (t, 4H, J = 6.9 Hz), 4.27 (t, 0.6H, J = 10.5 Hz), 3.94 (t, 4H, J = 5.7 Hz), 3.03 (s, 0.6H), 2.90 (s, 0.9H), 2.86 (s, 0.4H), 2.08 (m, 4H), 1.86 (m, 5H), 1.42 (m, 3H), 1.00 (m, 0.2H), 0.70 (m, 0.6H). ^{13}C NMR (75 MHz, $CDCl_3$, ppm): δ 166.4, 166.3, 159.8, 140.3, 137.7, 137.0, 136.2, 132.4, 132.2, 125.7, 122.9, 120.4, 118.8, 108.6, 107.8, 106.1, 69.2, 68.5, 67.8, 49.4, 45.0, 44.0, 43.7, 42.7, 42.2, 41.6, 38.0, 37.8, 29.6, 29.0, 26.9, 25.8. MS (MALDI-TOF) Calcd. for $[C_{47}H_{46}N_2O_4]^+$: m/z 702.35. Found: m/z 702.59 $[M + H]^+$.

Synthesis of Bicyclo[2.2.1]hept-5-en-2-ylmethyl 3,5-Bis(3,5-bis(4-(9H-carbazol-9 yl)butoxy)benzyloxy)benzoate (*Nb-G2*). In a 100 mL round-bottom flask equipped with a stirrer bar and an addition funnel, a solution of G2COOH (0.69 g, 0.54 mmol),

(72) Kaewtong, C.; Jiang, G.; Felipe, M. J.; Pulpoka, B.; Advincula, R. *ACS Nano* **2008**, *2*, 1533.

5-norbornene-2-methanol (mixture of endo and exo) (0.074 g, 0.59 mmol), and DMAP (7.3 mg, 0.059 mmol) in 10 mL of dry CH_2Cl_2 was cooled to 0 °C under N_2. DCC (0.122 g, 0.59 mmol) was dissolved in 5 mL of CH_2Cl_2 and added dropwise to the reaction flask under stirring. After complete addition of DCC, the reaction was stirred for 10 min at 0 °C and then allowed to stir at room temperature overnight. Then, the white solids were removed by gravity filtration, and the filtrate was washed with dilute sodium bicarbonate (20 mL) and water (2 × 20 mL) and finally dried over anhydrous Na_2SO_4. The solution was filtered, and the solvent was removed to yield the white crude product mixture, which was further purified by column chromatography on silica gel using 4:1 CH_2Cl_2/hexane as the eluent. The final yield was 0.33 g (43.8%). ^{1}H NMR (300 MHz, $CDCl_3$, ppm): δ 8.14 (d, 8H, J = 7.5 Hz), 7.53−7.41 (m, 16H), 7.34−7.22 (m, 8H), 6.81 (s, 1H), 6.55 (d, 4H, J = 1.8 Hz), 6.36 (s, 2H), 6.20 (q, 0.6 H, J = 3.0 Hz), 6.12 (m, 0.8 H), 6.00 (q, 0.6 H, J = 3.0 Hz), 5.00 (s, 4H), 4.41 (t, 8H, J = 6.9 Hz), 4.16 (m, 1.4H), 3.93 (t, 8H, J = 6.3 Hz), 2.96 (s, 0.6H), 2.86 (s, 0.9H), 2.80 (s, 0.4H), 2.52 (m, 0.6H), 2.09 (m, 9H), 1.85 (m, 11H), 1.31 (m, 13H), 0.92 (m, 5H), 0.65 (m, 1H). ^{13}C NMR (75 MHz, $CDCl_3$, ppm): δ 166.6, 160.9, 160.3, 140.9, 139.4, 138.1, 137.4, 136.8, 133.1, 132.7, 131.3, 126.2, 123.5, 120.9, 119.4, 109.1, 107.6, 106.6, 101.6, 70.8, 69.7, 69.0, 68.2, 53.9, 49.9, 45.6, 44.5, 44.3, 43.2, 42.8, 42.2, 32.4, 30.2, 29.5, 27.5, 26.3, 23.1. MS (MALDI-TOF) Calcd. for $[C_{93}H_{88}N_4O_8]^+$: m/z 1388.66. Found: m/z 1388.68 $[M + H]^+$.

2.4. General Polymerization Procedure. ROMP of the dendritic monomers was conducted under N_2 atmosphere at room temperature over 16 h in THF. The feed ratio of the monomers and Grubbs' first-generation catalyst was 50:1 and 200:1. The polymerization was terminated by adding a large excess of ethyl vinyl ether, and after 30 min the reaction was stopped and the solvent was evaporated. The crude polymer was redissolved in minimum amount of THF and reprecipitated in hexane or methanol. The dispersion solution was then centrifuged for 10 min at 4400 rpm. This reprecipitation procedure was repeated at least three times to completely remove the impurities as monitored by ^{1}H NMR. The white polymers were then dried and stored in vacuum oven before characterization. Typical yield of the polymers was 84%−95%.

2.5. Intrapolymer Cross-Linking by $FeCl_3$ Oxidation. A concentration 0.01 mg/mL of PNbG2-200 solution in $CHCl_3$ was prepared, and $FeCl_3$ chloroform solution was added dropwise into the PNBG2-200 solution under gentle stirring and N_2 protection. The molar ratio of $FeCl_3$ to carbazole monomer was set as 50:1. The reaction was monitored with UV−vis spectroscopy by observing the polaronic and bipoloronic peaks due to the extension of carbazole conjugation. The reaction was stopped after 48 h, and during the reaction process chloroform was added frequently to maintain a constant reaction concentration.

3. Results and Discussion

3.1. Synthesis of Terminal Carbazole Dendronized Norbornene Macromonomers and Polymers. Electrically conducting and π-conjugated polymers used for the fabrication of optoelectronic devices are generally synthesized by polycondensation or anodic electropolymerization methods. To avoid aggregation and improve solubility of such materials, side chains, primarily alkyl groups, have been attached to the monomer prior to polymerization.[73,74] The polymers prepared by these methods normally end up with broad polydispersities and the polymerization process poorly controlled. By taking advantage of living ROMP which allows for precise control over polymer chain length (MW) and PDI, we aimed to synthesize electroactive

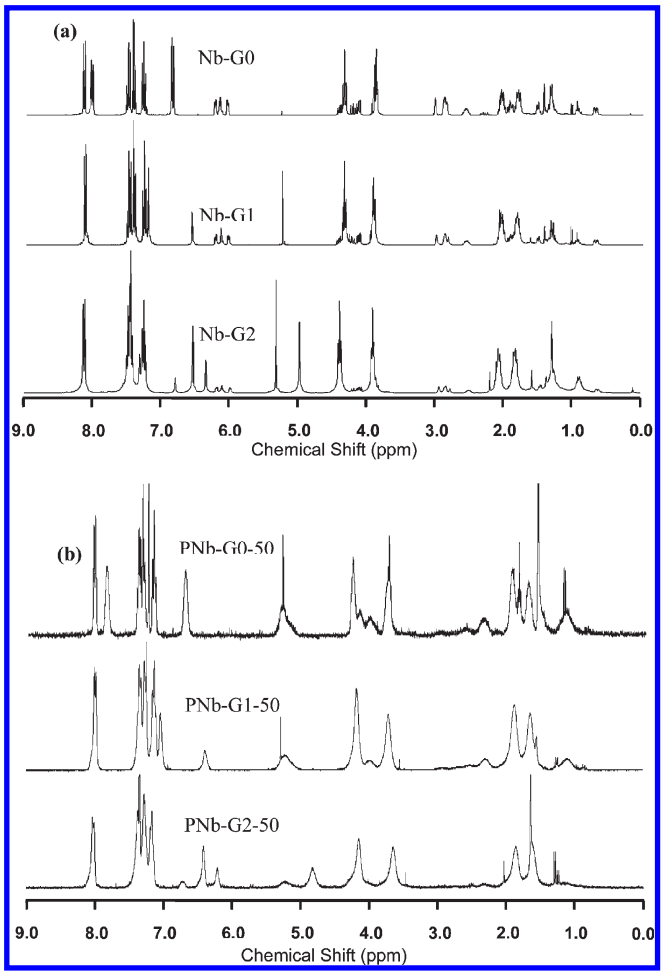

Figure 1. ^{1}H NMR spectra in $CDCl_3$ of monomers (a) and polymers (b) with different generations of the dendron pendant groups.

dendronized polymers via a macromonomer route. To the best of our knowledge, there have been no reports on the synthesis of DLPs bearing electroactive dendron with carbazole side groups. The norbornenyl dendrons were synthesized via esterification from commercially available 5-norbornene-2-methanol (endo/exo mixture) and terminal carbazole dendron carboxylic acids with different generations (G0COOH, G1COOH, and G2COOH). The reactions were conducted in the presence of DCC and DMAP under mild conditions. The norbornenyl macromonomers have been proven to be easily polymerized by ROMP using Grubbs' catalysts.[75,76] As shown in Figure 1a, the characteristic resonances of the norbornenyl alkene protons in the ^{1}H NMR spectra were observed at 6.0−6.2 ppm. After the ring structure was opened with polymerization, these peaks disappeared. The appearance of a new broad peak centered at 5.2 ppm was observed due to protons of the opened ring polymer main chain.[21,76,77] The feed ratio of the monomers and first generation Grubbs' catalyst was chosen as 50:1 or 200:1 in an attempt to control the MW of the dendronized polynorbornenes. The resulting polymers were found to be very soluble in most common organic solvents, such as THF, CH_2Cl_2, $CHCl_3$, and acetonitrile. The MWs and PDIs calculated from the GPC results are summarized in Table 1. As expected, the experimental MWs

(73) Malenfant, P. R. L.; Fréchet, J. M. J. *Macromolecules* **2000**, *33*, 3634.
(74) Krishnamoorthy, K.; Ambade, A. V.; Mishra, S. P.; Kanungo, M.; Contractor, A. Q.; Kumar, A. *Polymer* **2002**, *43*, 6465.
(75) Nyström, A.; Malkoch, M.; Furó, I.; Nyström, D.; Unal, K.; Antoni, P.; Vamvounis, G.; Hawker, C.; Wooley, K.; Malmström, E.; Hult, A. *Macromolecules* **2006**, *39*, 7241.
(76) Patton, D. L.; Advincula, R. C. *Macromolecules* **2006**, *39*, 8674.
(77) Cheng, C.; Khoshdel, E.; Wooley, K. L. *Macromolecules* **2007**, *40*, 2289.

Table 1. Number Average Molecular Weights (M_n) of Theoretical and Experimental Values, Monomer Repeat Units Calculated from the Experimental M_n, and Polydispersity Indices (PDIs) of the Dendronized Polymers

polymers	$M_{n,theory}$ (KDa)	$M_{n,GPC}$ (KDa)	repeat units	PDI
PNbG0-50	23.3	26.5	57	1.13
PNbG0-200	93.2	89.2	192	1.14
PNbG1-50	35.2	44.8	63	1.23
PNbG1-200	140.6	150.3	213	1.28
PNbG2−50	69.5	66.6	48	1.24
PNbG2-200	278.0	243.6	175	1.40

Table 2. Thermal Properties of the Dendronized Polymers by Thermogravimetric Analysis (TGA) and Differential Scanning Calorimetry (DSC)

polymers	T_d (°C) (5% weight loss)	T_g (°C)
PNbG0-50	349	85.8
PNbG0-200	365	85.3
PNbG1-50	394	84.6
PNbG1-200	400	83.5
PNbG2-50	355	81.8
PNbG2-200	379	80.9

obtained were mostly in good correlation with the theoretically calculated values. The chain length of PNbG2-200 was slightly shorter than expected. This might be related to the steric effect for the bulky dendron, leading to a relatively lower degree of polymerization. The dendronized polynorbornenes were synthesized, in most cases, with PDIs of 1.1 or 1.2, which is one of the indicators for a living/controlled polymerization of the dendrons via ROMP. The polymers with the lower generation dendrons (G0 and G1) showed better PDIs, while the polymers with the G2 dendron gave broader distributions. Again, this is a consequence of the steric effect reducing access to norbornene units of the bulkier G2. Solubility is not expected to be a factor, since all the dendrons are totally soluble to the polymerization solvent.

3.2. Thermal Properties of the Dendronized Polymers. The thermal properties in terms of polymer decomposition temperature (T_d) and glass transition temperature (T_g) are summarized in Table 2, as investigated by TGA and DSC, respectively. One of the major concerns for real application of organic/polymeric materials is their thermal stability. In this present study, the T_d at the first 5% weight loss spanned from 350 to 400 °C, better than most linear vinylic polymers which is usually at 250−300 °C. This good thermal stability should hold promise for more thermo-mechanically demanding applications. As can be seen from Table 2, PNb-G0 exhibited the lowest T_d while PNb-G1 showed the highest T_d and PNb-G2 was found in between. The reason for this trend is unclear but may be related, but not limited, to the minimum energy conformation of the dendron side group within the main chain influencing depolymerization. The glass transition temperature (T_g) of the dendronized polymers was determined from the second heating DSC run and taken as the middle point of the transition. The T_g's of the polymers are at the 80−86 °C range. It is clear that the T_g of the polymers decreased as the dendron size increased. The T_g of polynorbornene without side groups is 215 °C, which is significantly higher than that of the terminal carbazole dendronized polymers. It can be explained considering that larger dendritic pendants result in amorphous structures because of poor chain−chain packing behavior. By comparison, the dendronized polynorbornenes bearing acetonides[21] exhibited even lower T_g ranging from 18 to 33 °C. This may be attributed to the absence of the more rigid aromatic rings on these dendron side groups. In addition, the T_g of the polymers with the same generation dendrons was found almost the same.

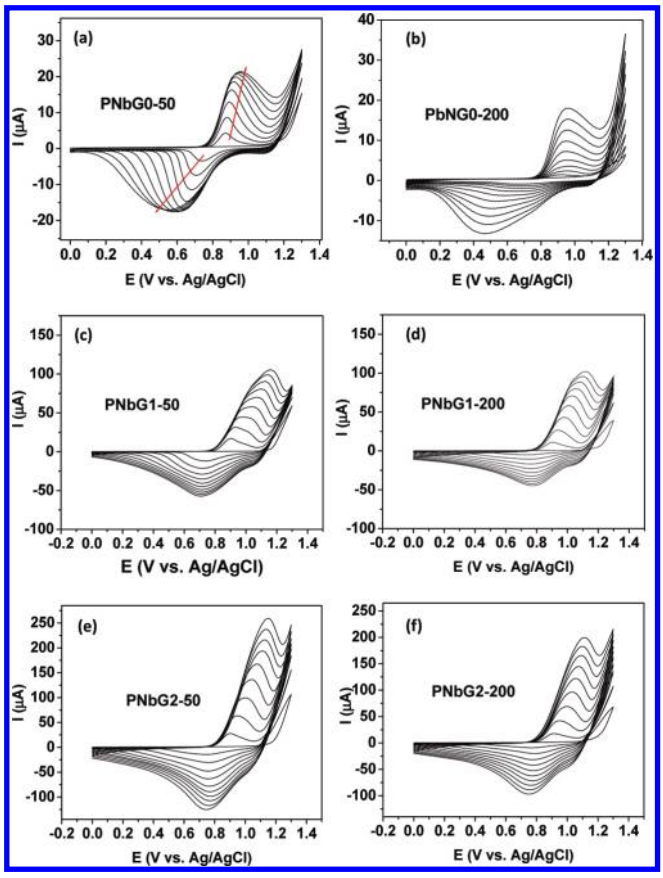

Figure 2. Cyclic voltammograms from PNbG0-50 (a), PNbG-200 (b), PNbG1-50 (c), PNbG1-200 (d), PNbG2-50 (e), and PNbG2-200 (f). All the polymer solutions were 1 mM based on each monomer repeat unit. The supporting electrolyte solution was prepared with 0.1 M tetrabutyl ammonium hexafluorophosphate ($TBAPF_6$) in THF. Scan rate was 50 mV/s. Arrows in (a) indicate from 1st to 10th cycle for clarity, and they apply to all other figures.

3.3. Electrodeposition and Electrochemical-QCM Study of the Dendronized Polymers. The electrochemical cross-linking of carbazole pendant precursor polymers has been studied by our group for some time.[48−54] The mechanism is shown in the Supporting Information, SI Figure 5. By coupling an electrochemistry setup with a QCM, it is possible to simultaneously investigate the electrochemical cross-linking behavior of the terminal carbazole dendronized polymers and record nanogravimetric changes occurring at the interface of gold electrodes during deposition.[53,76] In all cases of the electrochemical deposition of these polymers, 10 cyclic voltammetry (CV) cycles were applied by scanning the electrodes from 0 to 1.3 V. The concentration of the polymers was 1 mM in THF based on the monomer unit. All the CV results are shown in Figure 2, with the arrows pointing from the first to 10th cycle. On the first CV cycle from all the polymers, the onset of the carbazole oxidation was found at ~1.1 V. Starting from the second CV cycles, the oxidation waves ranged from 0.7 to 1.2 V, which originates from the doping of the polymerized carbazoles and formation of polaronic and bipolaronic species. The reduction peaks from 1.0 to 0 V corresponded to the dedoping process, in which the polarons and bipolarons gained electrons to give the neutral coupled carbazole species. Carbazole-based polymers for fabrication of electrochromic devices highly rely on this electrochemically induced doping−dedoping property.[49] Upon further cycling, the oxidation

Table 3. Anodic, Cathodic Peak Potentials, Currents, Peak Separations, and Corresponding Onsets of the Oxidation Waves from the Dendronized Polynorbornenes

polymers	onset (V)	E_{pa} (V)	E_{pc} (V)	ΔE (V)	i_{pa} (μA)	i_{pc} (μA)	thickness (nm)
PNbG0-50	0.70	0.96	0.55	0.41	21.5	−17.1	85.3 ± 6.4
PNbG0-200	0.69	0.96	0.46	0.50	18.1	−13.3	91.0 ± 7.2
PNbG1-50	0.70	1.17	0.71	0.46	105.1	−57.6	189.6 ± 12.2
PNbG1-200	0.71	1.12	0.77	0.35	101.3	−44.6	193.1 ± 11.7
PNbG2-50	0.72	1.16	0.74	0.42	258.5	−125.3	255.4 ± 15.1
PNbG2-200	0.72	1.11	0.75	0.36	199.0	−96.7	243.7 ± 13.3

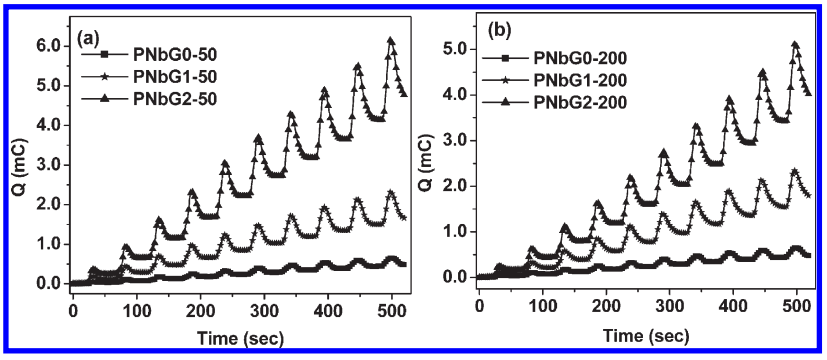

Figure 3. Amount of charge (Q) as a function of time during electropolymerization of the different polymers.

and reduction currents increased progressively, indicating a continuous mass deposition of the polymers with more charges built up in the electropolymerized films. Meanwhile, the anodic and cathodic peaks moved further apart with increasing CV cycles, more apparently from polymers with higher generation dendron side groups. This suggested that heterogeneous electron transfer became more predominant as more polymers were electrochemically deposited onto the electrodes. The redox peak potentials and currents were found to be comparable from polymers coupled with the same dendron generation, regardless of the polymer MW. Table 3 summarizes the CV results and thin film thicknesses based on the 10th cycle, including the onsets of the polymer oxidation, anodic and cathodic peak potential (E_{pa} and E_{pc}), peak separation (ΔE), as well as the anodic and cathodic currents (i_{pa} and i_{pc}). According to the ratio between i_{pa} and i_{pc}, the CV waves were more reversible for PNbG0-50, while the polymers with higher generation dendrons displayed more irreversible couples. In addition, the anodic and cathodic currents from PNbG0-50 and PNbG0-200 were significantly lower than those from the higher generation dedronized polymers.

The cross-linking efficiency of the polymers can be characterized by determining the ratio of the overall charge (Q) in the films to the thickness of the electropolymerized films (d). Figure 3 shows the total amount of charges (Q_t) building up in the electropolymerized films during the cross-linking process. The values of 9.27×10^{-6}, 1.86×10^{-5}, and 1.65×10^{-5} C/nm were determined with increasing dendron size. It is evident that, during electropolymerization, the polymers with higher generation dendrons exhibited the greater cross-linking efficiency, that is, the presence of more carbazole units. This suggested that effective π-conjugation of the carbazyls is still possible, overcoming any conformational restrictions that may be present, being tethered in a linear polymer backbone especially with the second generation carbazole dendrons. This is in contrast to the decrease in electrochemical cross-linking efficiency and π-conjugation of globular higher generation dendrimers, with G-4 bearing peripheral carbazole groups as previously investigated by our group.[68]

In the QCM measurement, the change in mass (Δm) is related to the change in the fundamental resonance frequency (ΔF) of the QCM crystal by the well-known Sauerbrey equation.[78] However, this model is only valid when (1) the adsorbed films are rigid, (2) the frequency shift due to the mass deposition is negligible by comparing with resonant frequency of the bare QCM crystal, and (3) the measurement is carried out in air or under vacuum. In our case, electropolymerization of the dendronized polymers was performed in THF. Thus, the contribution to the frequency shifts from the viscoelasticity of the polymers and the solvent viscosity have to be taken into consideration. Kanazawa established a new model in which the solvent density and viscosity were both included.[79] The viscoelastic properties of the polymers can be studied by impedance analysis based on the Butterworth−van Dyke (B-VD) equivalent circuit. The circuit element motional resistance R in the B-VD model provides the information about the dissipation factor or energy loss due to the damping process in a viscoelastic system. Therefore, a change in ΔR predicts a change in viscoelasticity of the polymer films adjacent to the electrode surface. A smaller change in ΔR is correlated to a more rigid film deposition. By monitoring ΔR as a function of frequency change, in principle we can determine the relative shear viscosity and elastic modulus of the electropolymerized films.[68]

As shown in Figure 4, the frequency shift with each CV cycle was monitored as a function of electropolymerization time or number of CV cycles. During each CV cycle, the polymer deposition onto the surfaces was followed. A partial dissolution of the deposited polymers into the solvent was also observed. This is also indicative of the doping and dedoping process during the electrochemical cross-linking. Similar to the CV results, the frequency shift seemed to be largely independent of the polymer chain length. The frequency change (ΔF) increased with increasing dendron generation, in both cases for low and high polymer MW. In most of these investigations, frequency changes (ΔF) were interpreted in terms of rigid mass changes, based on the Sauerbrey equation. For thin films (where the film thickness is much less than the wavelength of the piezo-electrically launched shear waves), a modified Sauerbrey equation is used to convert

(78) Sauerbrey, G. *Z. Phys.* **1959**, *155*, 206.
(79) Kanazawa, K. *Faraday Discuss.* **1997**, *107*, 77.

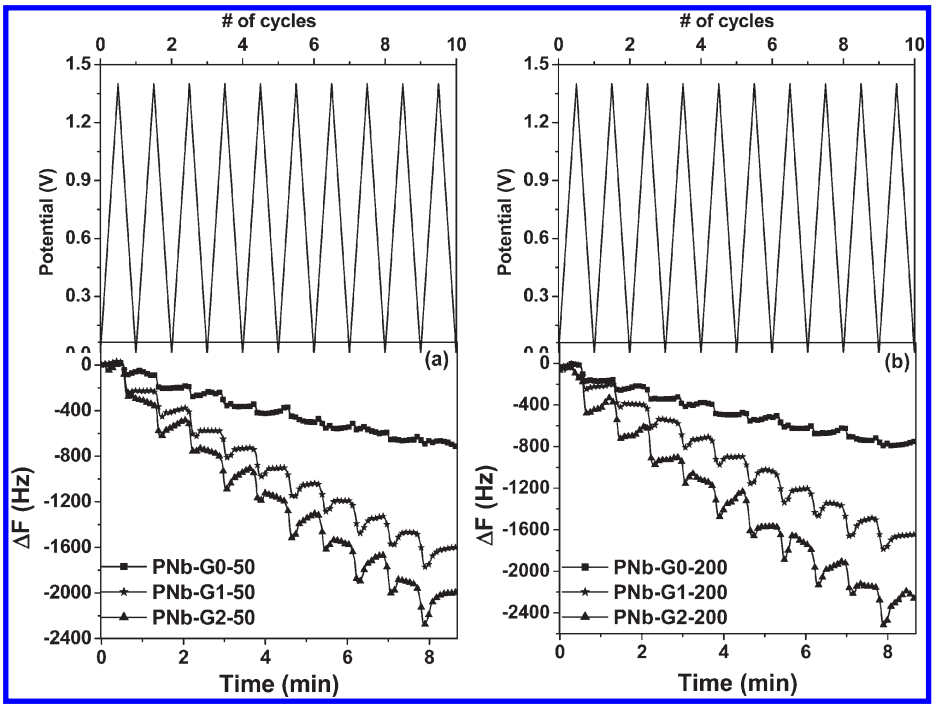

Figure 4. QCM frequency shifts as a function of electropolymerization time and CV cycles.

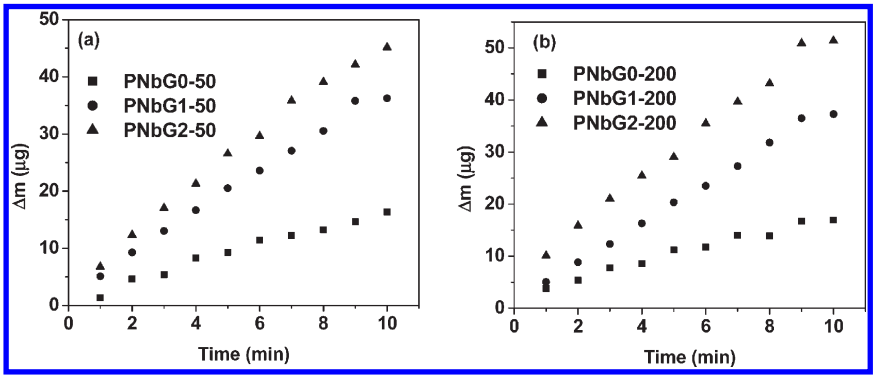

Figure 5. Calculated mass change after each CV cycle as a function of electropolymerization time for the different polymers.

ΔF to mass changes (Δm).[80] A change in Δm on the working electrode during the formation of the cross-linked polymer films as a function of electropolymerization time is shown in Figure 5

Figure 6 shows the QCM resonance resistance change at the dedoped state as a function of the frequency change for the CV deposition of all the dendronized polynorbornenes. It can be clearly seen that the polymers with the lowest generation dendrons, regardless of polymer chain length, exhibit a smaller resistance shift during the whole course of the electropolymerization process. While upon increasing dendron generation, the resistance change turned out greater. Meanwhile, for both G1 and G2 carbazole dendronized polynorbornenes, the resistance changes show a continuous increase with increasing frequency shift. These results reveal that the electropolymerized films become more viscoelastic or less rigid with increasing dendron generation. This is another strong support that the cross-linking efficiency increases with higher dendron generation for these polymers, leading to an increase in free volume with the polymer films, as discussed above by comparing the ratios (Q_t/d) between the overall charge and the film thickness. This observation is similar to the dendrimeric structures constructed from terminal carbazole dendrons, except for the much higher and crowded G4 dendrimer.[68] Overall, the electrochemical behavior in terms of the redox potential and current, the electro-cross-linking efficiency, and the viscoelasticity are correlated with the differences in conformational properties and free volume of the dendron side groups in the linear polynorbornenes.

The surface morphology of the electropolymerized films was examined by tapping-mode AFM imaging. As shown in Figure 7, the size of the globular shaped features increases from the lowest generation dendronized polymers to the highest ones. The difference in the feature size may be related to differences in polymer nucleation and aggregation during the electropolymerization process. On the other hand, the contribution from the size of the polymers itself should also be taken into consideration. That is to say, even if the polymers have the same level of nucleation and aggregation, the highest generation dendronized polymers are expected to form bigger aggregates which readily accumulate on top of the electrodes as is the case. The calculated surface roughness of the electropolymerized films from Figure 7a to f were 8.8, 13.4, 16.4, 38.9, 29.3, and 23.2 nm.

3.4. Nanoparticle Formation: Size and Shape Control Study of PNbG2-200. One of the most interesting features of

(80) Baba, A.; Tian, S.; Stefani, F.; Xia, C.; Wang, Z.; Advincula, R.; Johannsmann, D.; Knoll, W. *J. Electroanal. Chem.* **2004**, *562*, 95.

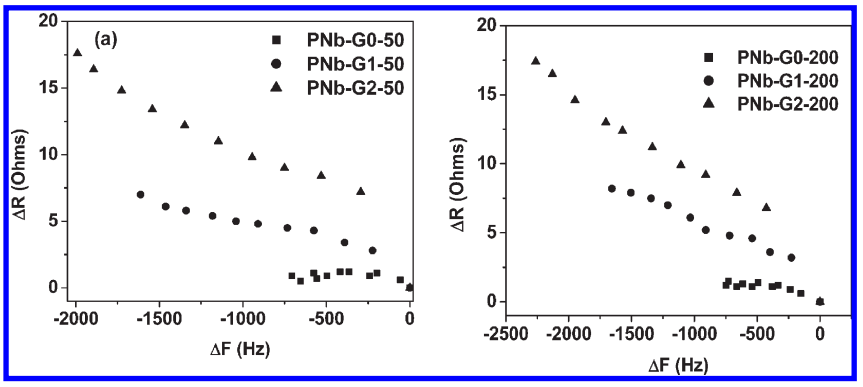

Figure 6. Change in resonance resistance as a function of the change in frequency during the CV electropolymerization of the different polynorbornenes.

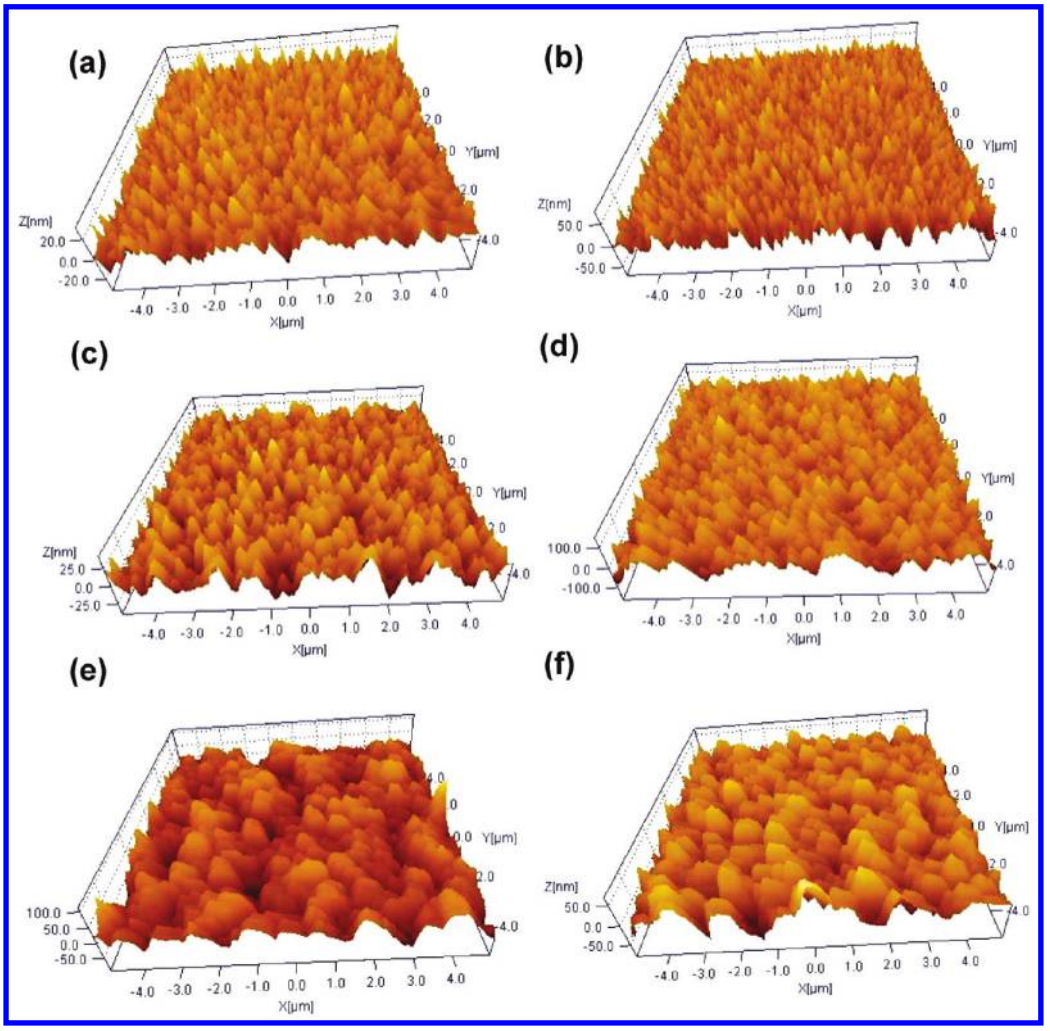

Figure 7. AFM 3D topographic images of the electropolymerized films from PNbG0-50 (a), PNbG-200 (b), PNbG1-50 (c), PNbG1-200 (d), PNbG2-50 (e), and PNbG2-200 (f).

dendronized polymers is their shape dependence on dendron generation and grafting density. It has been well documented that, with increasing dendron generation, the persistence length of polymer backbone increases accordingly.[81] Thus, we are particularly interested in the polymer with highest generation and longest chain length, which is PNG2-200. When the PNbG2-200 solutions with different concentrations (0.001, 0.01, and 0.1 mg/mL) were spin coated onto freshly cleaved mica surfaces, nanospherical particles of almost monodispersed distribution in size was observed. Figure 8 shows the 2D and 3D AFM images which were obtained under tapping mode on the spin-cast films (3000 rpm and 90 s) from increasing solution concentration. It is obvious that this polymer aggregates to form nanospheroidal shapes, minimizing the interaction with the hydrophilic mica.[27] The average height of the particles was found to be 6.1 ± 1.5, 9.2 ± 0.7, and 20.5 ± 2.1 nm (based on

(81) Das, J.; Fréchet, J. M. J.; Chakraborty, A. K. *J. Phys. Chem. B* **2009**, *113*, 13768.

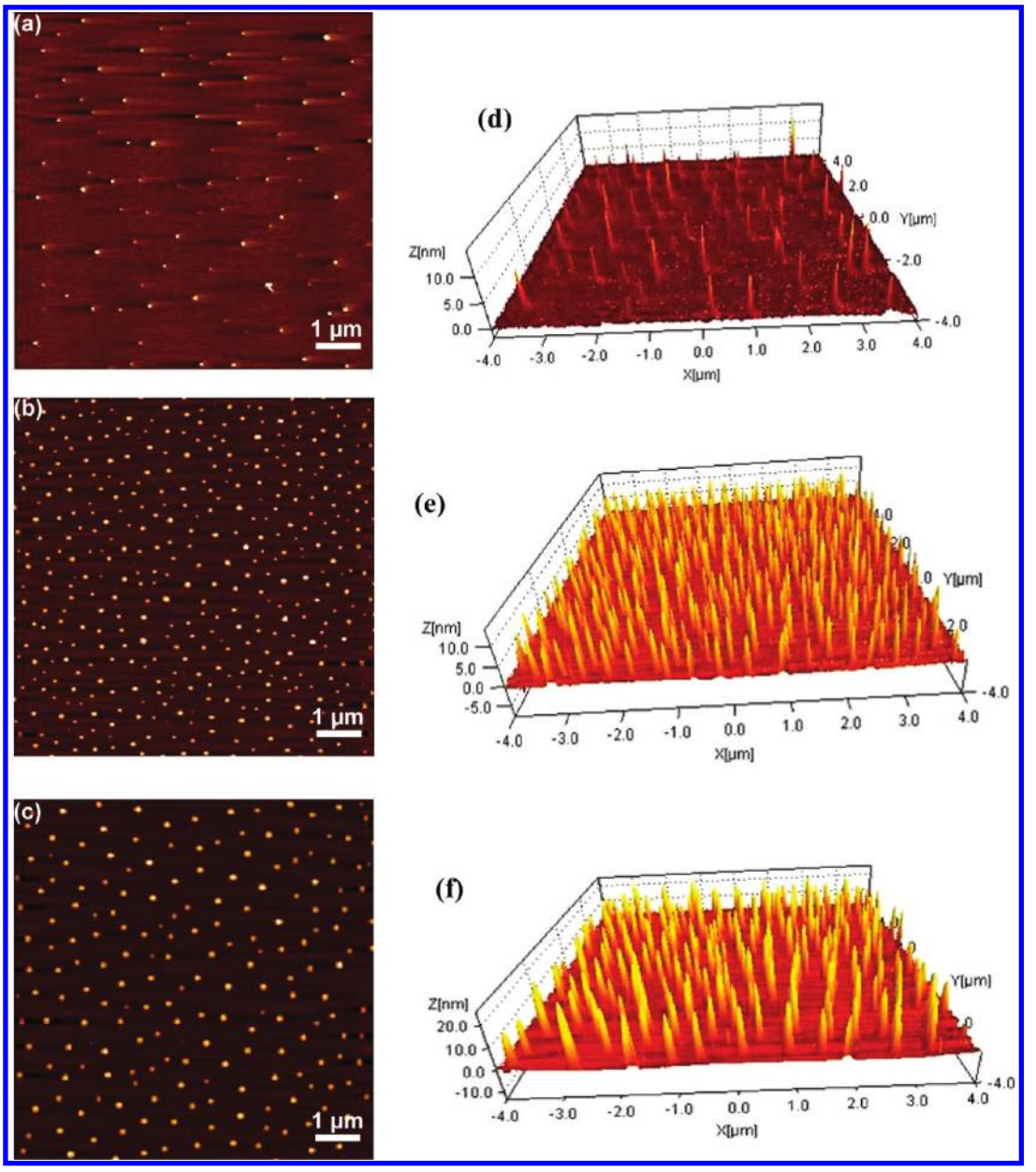

Figure 8. 2D and 3D images of spin-cast films from PNbG2-200 with a concentration of 0.001 mg/mL (a, d), 0.01 mg/mL (b, e), and 0.1 mg/mL (c, f).

image height histogram) with increasing concentration. However, the absolute diameter of the domains cannot be quantitatively determined due to the inherent tip convolution effect with the AFM method. It is not clear how many polymer chains are included per particle at this point. Nevertheless, there is an observable trend in that the size expands with increasing concentration, owing to increased unit aggregation. Modification of the mica substrate with hexadecyltrimethoxysilane (HDTMS) provided a more hydrophobic surface. HDTMS (1 mM) in toluene was prepared, and freshly cleaved mica substrates were immersed in the silane solution at 70 °C up to 24 h. The static water contact angle (WCA) changed from 5° with bare mica to 95° after functionalization (see Supporting Information SI Figure 1a). The AFM image (Supporting Information SI Figure 1b) showed there were still a few defects/holes over the monolayer film. The AFM profilometry study (Supporting Information SI Figure 1c) found that the depth of the holes was comparable to a monolayer film thickness. Regardless of the defects, the baseline from the profilometry was found to be very smooth, which was important to interpret further studies. Compared to the exclusively spheroidal domains on the freshly cleaved mica (Figures 8b and 9a), at a relatively lower concentration (0.01

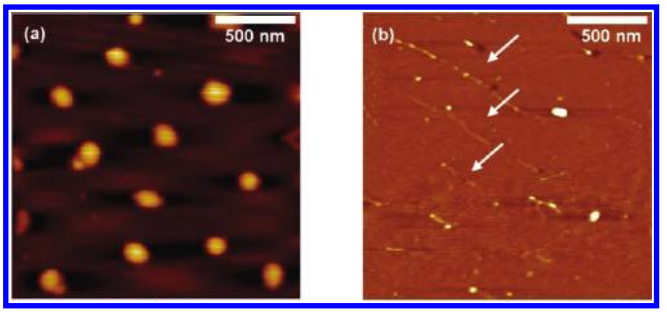

Figure 9. 2D Tapping-mode AFM images ($2 \times 2\,\mu m^2$) of spin-cast films from 0.01 mg/mL PNbG2-200/$CHCl_3$ solution on mica (a) and HDTMS-modified mica (b). Arrows point to extended polymer chains on the wettable hydrophobic substrate.

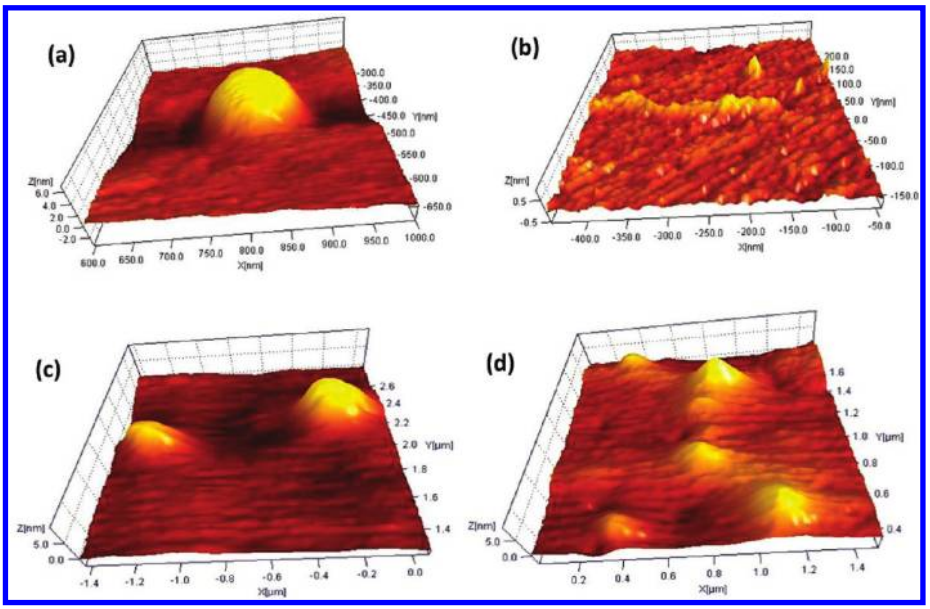

Figure 10. 3D Tapping mode AFM images (magnified) of spin-cast films from (a) 0.01 mg/mL PNbG2-200/$CHCl_3$ solution on bare mica, (b) 0.01 mg/mL PNbG2-200/$CHCl_3$ solution on HDTMS-modified mica, (c) 0.01 mg/mL chemically cross-linked PNbG2-200/$CHCl_3$ solution on bare mica, and (d) 0.01 mg/mL chemically cross-linked PNbG2-200/$CHCl_3$ solution on HDTMS-modified mica.

mg/mL), rodlike nano-objects (Figure 9b) were observed on the hydrophobic monolayer covered mica surface via spin-coating. Some features were found to "connect" or "stack" with each other, forming longer rods up to 1 μm, as evidenced by the brighter dots among the individual polymers. However, there were still some spheroidal objects on the surfaces, because the monolayer-covered surface was not completely hydrophobic. Compared to the spheroidal objects on the freshly cleaved mica surface (Figure 9a), the size of the spheroidal objects in Figure 9b is much smaller. This proves that the extent of aggregation of the dendronized polymers is lower on the hydrophobically modified mica. Further modification of the mica surface with even more hydrophobic monolayer films may improve the quality and increase the amount of the rodlike nanofeatures. AFM profilometry analysis suggested that these rodlike objects are comparable to the typical height of individual polymer chains extended on the surface, with a height of 0.7 $\pm$ 0.1 nm. Leaving the solution for a period of time (20 days), the polymers aggregated to some extent without changing the domain height (Supporting Information SI Figure 2a). The use of higher concentration PNbG2-200 solution (0.1 mg/mL) on the hydrophobic mica surface did not yield well-defined rodlike shapes however. Instead, the smaller spheres spread out the whole surface in a more random fashion with very few cylindrical objects. Interestingly, some of the particles connected to each other, forming considerably long pearl-necklace-like objects (Supporting Information SI Figure 2b). Studies on the morphology of the spin-coated PNbG2-200 solution (0.01 mg/mL) onto thermally evaporated gold surface with different surface wetting properties were also investigated, resulting in circular and wormlike morphologies (Supporting Information SI Figure 3). The above preliminary results suggest that further studies should be attempted using atomically flat Au(111) as the substrate, which would be ideal both for formation of the well-defined spheroidal or rodlike shapes and for electrochemical cross-linking of the objects by conducting AFM.

Chemical/electrochemical oxidation of the carbazole cross-linkers allowed for the formation of CPNs in the form of nano-objects.[67] This electrochemical or oxidative chemical cross-linking would result in a shrinkage of hydrodynamic volume of each individual polymer or nano-object and result in more rigid mechanical properties (Scheme 2). In this study, an ultradilute PNbG2-200 solution (0.01 mg/mL in $CHCl_3$) was subjected to chemical oxidation with $FeCl_3$. The molar ratio of $FeCl_3$ to carbazole monomer was set as 50:1. The ultralow concentration was used to avoid aggregation and interchain oxidation as much as possible, but it is expected to form particles as shown by AFM. UV−vis spectroscopy was used to first monitor the chemical oxidation of the dendronized polymer (Supporting Information SI Figure 4). A shoulder peak centered at ~375 nm appeared, indicating the formation of an extended π-conjugation of the carbazole units, consistent with previous studies.[67] In addition, two peaks centered at ~440 and 630 nm can be attributed to the formation of polycarbazole and the polaronic and bipolaronic bands, which were not previously observed in an earlier report regarding the intramolecular oxidation of the G3 carbazole dendrimers.[67] This property may well be unique for this dendronized linear polymers compared to dendrimers.

Scheme 2. Chemical Oxidation or Electrochemical Oxidation Induced Intrapolymer Cross-Linking

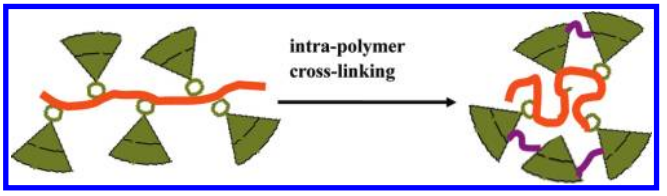

The macromolecular conformation effect on the degree of local oxidation toward different conjugation lengths, that is, intramolecular exciton migration, may be the main reason. Finally, the chemically cross-linked PNbG2-200 solution was spin-coated onto bare mica and HDTMS-modified mica surfaces. As shown in Figure 10, the polymer aggregation on the surfaces is visibly different. The cross-linked polymers on bare mica assembled in a more independent fashion than those on HDTMS-modified mica surfaces. However, spheroidal nano-objects were formed in both cases, with larger domains on bare mica and smaller ones on HDTMS-modified mica due to more spreading. This is in

contrast to the un-cross-linked polymers (Figure 9). Accordingly, the height of the domains was estimated to be 8.2 ± 1.8 and 5.1 ± 1.2 nm from Figure 10c and d. This difference reflects more on the wetting properties of the substrates which is better for the HDTMS-modified mica. Thus, upon intrachain (partially interchain) cross-linking, the polymers became more compact and rigid. Therefore, even on the hydrophobic mica surfaces, no rodlike objects were observed for the cross-linked PNbG2-200. Thus, the degree of the polymer conjugation via carbazole cross-linking directs assembly behavior, which might be an attractive feature for potential applications as conducting polymer nanoparticles for the fabrication of nanoelectronic devices and nano-objects.

Very recently, Das et al. reported the computational investigation on self-assembly of dendronized polymers.[81] Depending on dendron size and density, different phases ranging from lamellar to gyroid were predicted. While our present work focuses on individual polymer nanoparticle formation, further studies on self-assembly of the carbazole-dendronized polynorbornenes in bulk films and in solutions should enable us to take advantage of this type of polymers for nanotechnological applications.

4. Conclusions

In this paper, we reported the synthesis of a series of terminal carbazole dendronized polynorbornenes (up to G2) by ring-opening metathesis polymerization in the presence of the first generation Grubbs' catalyst. The macromonomer route was used to prepare the dendronized polymer materials. The polymer molecular weight (degree of polymerization) was controlled by varying the ratio between the monomer and initiator. With most of the polymers having narrow polydispersites (< 1.3), and the dependence of the MW on the dendron/catalyst feed ratio, the polymerization was proven to be a living process. The dendronized polymers were characterized by NMR, GPC, TGA, and DSC. The electrochemical behavior and the polymer film deposition on the gold electrodes were simultaneously recorded by E-QCM. Their electrochemical behavior in terms of redox peak position, current, reversibility, and electrochemical cross-linking efficiency was found to be largely dependent on the dendron generation. The viscoelastic property of the electrografted films was investigated by E-QCM and found to be correlated with the conformation of the side group on the polymers. To further investigate and better understand the steric effect of dendron generation on electropolymerizability and eventually nano-object formation on surfaces, higher generation dendrons (G3 or even G4) can be investigated. AFM was utilized to examine the surface morphology of the electropolymerized film. Nanoparticle formation was observed. In addition, the size and shape control of a selected polymer, PNbG2-200, was realized by varying the surface wettability or by intramolecular cross-linking via chemical oxidation. Thus, further investigation into structure−property correlation could help understand and further utilize these unique electroactive polymers in semiconductor device fabrication or nano-object synthesis.

Acknowledgment. The authors gratefully acknowledge the generous funding from the NSF DMR-10-06776, ARRA-CBET-0854979, CHE-1041300, Texas NHARP 01846, and Robert A. Welch Foundation, E-1551. C.D.G. thanks the Instituto Colombiano de Investigaciones Cientificas, COLCIENCIAS and Centro de Excelencia en Nuevos Materiales (CENM) for financial support through a doctoral fellowship. We also acknowledge technical support from Inficon Inc., Biolin (KSV Instruments), and Agilent Technologies.

Supporting Information Available: Water contact angle images, AFM image of hydrophobic silane covered mica surface, AFM images of PNbG2-200 spin coated on hydrophilic and hydrophobic gold substrates, and UV−vis spectra of PNbG2-200 before and after chemical cross-linking. This material is available free of charge via the Internet http://pubs.acs.org.